Differential cross sections for dissociative attachment in CO

R. I. Hall, I. Čadež,* C. Schermann, and M. Tronc†
Laboratoire de Physique et Optique Corpusculaires,‡ Université Pierre et Marie Curie, Tour 12, E. 5, 4 Place Jussieu, 75230 Paris, France
(Received 28 June 1976)

An electron-impact spectrometer is described which, by means of a modification, is able to observe energy and angular distributions of ion fragments produced by molecular dissociation processes with a good precision and sensitivity. O^- ion formation through dissociative electron capture in CO has been studied. An analysis of the observed O^- differential cross sections using the theory of O'Malley and Taylor and two partial waves indicates that the two reactions leading to O^- both proceed through a $^2\Pi$ resonant state. Both resonances appear to have a $\sigma^2\pi^3\pi^2$ configuration by analogy with isoelectronic NO, and their parents would be the $a'\,^3\Sigma^+$, for the process with a 9.62-eV threshold, and possibly the $d\,^3\Delta$ state, for the process with an onset at 10.88 eV.

I. INTRODUCTION

Negative-ion formation resulting from dissociative electron attachment has been repeatedly studied in electron-beam experiments since the first observations of Lozier[1] in 1930. In particular, these studies give information on the electron affinity of the fragments and on the potential-energy curve of the dissociating state.

If the dissociation energy D of the neutral diatomic molecule is known, then the electron affinity A of the negative-ion fragment can be determined from the measurement of its kinetic energy. Consider the dissociative attachment reaction

$$e + XY \rightarrow XY^- \rightarrow X + Y^- .$$

Then the excess reaction energy E is given by

$$E = E_0 - (D + E_n - A) ,$$

where E_n is the excitation energy of the fragments. E_0 is the kinetic energy available in the center-of-mass system and is essentially the incident electron energy measured in the lab since the electron mass is small compared to the molecular mass. If the target molecule is in its ground state, then E is shared between the fragments as kinetic energy. From energy and momentum conservation the residual energy E_R of the fragment is given by

$$E_R = (1 - \beta)[E_0 - (D + E_n - A)] , \qquad (1)$$

where $\beta = m/M$, m and M being the masses of the fragment and molecule, respectively. Thus the observation of the threshold for negative-ion production ($E_R = 0$) or a direct measurement of its kinetic energy leads to a knowledge of the electron affinity.

The observation of the dissociative attachment cross section as a function of electron energy is of value in determining the shape of the potential-energy curve of the intermediate negative-ion state. Also, a high-resolution study of the cross section can reveal fine structure due to interference effects which take place during the formation or dissociation of this state.

The first observations of negative-ion formation in CO were reported by Vaughan[2] and attributed to O^- ions. Since then dissociative attachment in CO has been studied by many workers, and a review of the literature has been presented by Chantry.[3] The dominant process for negative-ion formation through dissociative electron capture is

$$e + CO(^1\Sigma^+) \rightarrow CO^{-*} \rightarrow O^-(^2P) + C(^3P) , \quad \text{process I.}$$

The cross section peaks at threshold (9.62 eV), falls off slowly, and has a width at half maximum of about 1.2 eV. Rapp and Briglia[4] determined the maximum cross section to be 2.0×10^{-19} cm^2. A second process leading to O^- ions was observed by Chantry[3] through an energy analysis of the ions and is

$$e + CO(^1\Sigma^+) \rightarrow CO^{-*} \rightarrow O^-(^2P) + C^*(^1D) , \quad \text{process II.}$$

Here again the cross section was found to peak at threshold (10.88 eV), and Chantry[3] determined a maximum value of 9.5×10^{-21} cm^2, some 20 times smaller than for process I.

Other dissociative attachment processes, which yield C^- ions, were detected by Stamatović and Schulz.[5] The maximum cross section was found to be 6×10^{-23} cm^2 which made this process too weak to be studied in the present experiment.

As far as we are aware, no attempt has been made, either experimentally or theoretically, to determine the symmetries and configurations of the resonant states responsible for the formation of O^- ions. The present experiment was undertaken to obtain information of these subjects from observations of the dissociative attachment cross

section which are differential in scattering angle. Dunn[6] has pointed out that the angular distribution of the dissociation fragments of diatomics depends on the initial and final molecular states, and from symmetry arguments he developed selection rules which predict whether the differential cross section vanished or not when the molecule is orientated parallel or perpendicular to the incident electron beam. More recently O'Malley and Taylor[7] proposed an elaborate theory which gives expressions for the angular behavior of the differential cross section for diatomic molecules. This theory was used by Van Brunt and Kieffer[8] to interpret the angular distribution of negative ions formed by dissociative attachment in O_2.

In this paper we describe an experimental technique for observing negative-ion fragments which uses a conventional electron-impact spectrometer. This instrument has been modified by the addition of a magnetic-field momentum filter which effectively separates the electrons from the negative ions and, in this way, a fine study of the kinetics and geometry of the dissociative attachment process can be performed. The two processes, described above, which lead to O^- ion formation in CO, have been studied. Angular distributions for the O^- fragment have been compared to theory thus allowing symmetries and configurations to be proposed for the intermediate negative-ion states.

II. THEORY

Dissociative attachment is a particular case of resonant electron scattering where the intermediate negative-ion state dissociates before it can decay by electron ejection into a continuum. There is a competition between the dissociation and autoionization processes, and the latter is usually favored; resonance lifetimes being short compared to dissociation times. This results in small cross sections for dissociative attachment compared to those for resonant scattering.

The probability of an electron attaching depends on the symmetry of the resonant state to be formed and thereby on the orientation of the molecule. For diatomic molecules, the change in axial angular momentum of the molecular orbitals, as well as the parity for homonuclear diatomics, between the initial and resonant states determines the partial waves which can make up the resonance and determines also the probability that they will contribute to the attachment process as a function of the orientation of the internuclear axis. As the molecule dissociates along this axis then, the angular distribution of the fragments will reflect the probability of electron attachment as a function of the molecular orientation. Consequently, in an experiment where an electron beam defines an axis of symmetry, the observation of the angular dependence of the negative-ion fragment intensity in a plane containing the electron beam gives an insight into the symmetry of the intermediate negative-ion state. This is on condition that the molecule does not rotate appreciably during the lifetime of the resonant state, which, in the case of dissociative attachment, is determined by the dissociation time. If rotation does take place a general blurring of the angular distribution occurs. This effect can be accounted for, but is only important near the dissociation threshold where the fragment energies are of the same order as the rotational energies. In this study the measurements were not performed sufficiently close to threshold for this effect to be important.

According to O'Malley and Taylor,[7] and following their reasoning, the angular behavior of the dissociation products in the adiabatic approximation is determined by the electronic matrix element

$$V(\vec{R}) = \langle \phi_r \,|H_{el}\,| \phi_{ad} \rangle , \tag{2}$$

where H_{el} is the electronic Hamiltonian, ϕ_r is the electronic wave function of the resonant state, and ϕ_{ad} is the continuous adiabatic electronic wave function and can be written

$$\phi_{ad} = (1 + GV) e^{i\vec{k}\cdot\vec{r}_e} \phi_t(r_t, R) ,$$

where $e^{i\vec{k}\cdot\vec{r}_e}$ and ϕ_t and the wave functions of the free electron and the unperturbed target electronic state, respectively, G is a Green's function, and V is the interaction between the target molecule and the incident electron. The $GVe^{i\vec{k}\cdot\vec{r}_e}\phi_t$ term represents the distortion of the initial electronic state due to collision processes other than the interaction with the considered resonance.

It is through ϕ_{ad} that the orientation of the molecule enters into the expression for the transition probability, as $\vec{k}$ is referred to the molecular coordinate system. The incident plane wave in the molecular frame can be written

$$e^{i\vec{k}\cdot\vec{r}_e} = 4\pi \sum_{L=0}^{\infty} \sum_{\mu=-L}^{L} (i)^L Y^*_{L\mu}(\theta, \phi) \times Y_{L\mu}(\theta_e, \phi_e) j_L(k, r_e) ,$$

where j_L and $Y_{L\mu}$ are the Bessel function and spherical harmonic, respectively. When the above expression is inserted in Eq. (2), conservation of axial angular momentum places restrictions on the indices μ and L such that $\mu = \lambda_r - |\lambda_t|$, where λ_t and λ_r are the target and resonance axial angular momenta, respectively.

The general form of $V(\vec{R})$ is

$$V(\vec{R}) = (4\pi)^{1/2} \sum_{L=|\mu|}^{\infty} V_{L|\mu|}(R) Y^*_{L\mu}(\theta, \phi) .$$

For heteronuclear diatomic molecules, all values of $L \geq \mu$ are possible, but for homonuclear diatomics L is restricted to even or odd values depending on whether the initial and resonant states have the same or opposite parity. There is also the spin selection rule $S_r = S_t \pm \frac{1}{2}$, where S_r and S_t are the total spins of the resonant and target states, respectively. In addition there are restrictions on $\Sigma \rightarrow \Sigma$ transitions. As the wave function of an incident electron has "plus" symmetry, then reflection symmetry for these states in a plane containing the internuclear axis must be conserved. This imposes that only $\Sigma^+ \rightarrow \Sigma^+$ and $\Sigma^- \rightarrow \Sigma^-$ transitions can take place.

The differential cross section (DCS) for dissociative attachment can be written

$$\sigma(\theta, \phi, k) \sim \left| \sum_{L=|\mu|}^{\infty} a_{L,|\mu|}(k) Y_{L\mu}(\theta, \phi) \right|^2 , \qquad (3)$$

where $a_{L,|\mu|}$ are complex expansion coefficients. It is assumed that rotational effects are small, and that the following condition is satisfied:

$$E_R \gg \hbar^2 J(J+1)/2MR_0^2 ,$$

where J is the rotational quantum number, M is the reduced mass, R_0 is the internuclear distance, and E_R is the fragment energy given by Eq. (1). In this study, the observations are performed away from threshold, and the above condition is well borne out.

At low energies, few partial waves participate in the dissociative attachment process. O'Malley and Taylor[7] point out that the first allowed partial wave will dominate the reaction as expansion (3) converges rapidly due, firstly, to the form of the orbital of the attached electron and secondly, to the radial behavior of the partial-wave expansion of the incident electron wave function. If one partial wave alone is present, then only distributions which are symmetrical with respect to 90° can be obtained. If several partial waves are present, then parity restrictions in homonuclear diatomics impose symmetrical angular distributions here also. Distributions with forward-backward asymmetry are only possible in the heteronuclear case and with contributions from more than one partial wave.

Van Brunt and Kieffer[8] argue that forward-backward asymmetry could be introduced by an interaction between two resonant states. This can only be so for states of different symmetry and according to the selection rules of Kronig.[9] The coupling between the states is rotational and for such a dissociation process, involving small energies, it is reasonable to suppose that this is small, and that any asymmetry would necessarily be weak.

III. EXPERIMENTAL

In electrostatic fields, electrons and negative ions with the same energy follow the same path and, consequently, are present in spectra obtained by electron-impact spectroscopy. Except for special cases,[10] electrons are much more abundant and mask out any negative-ion features which may be present. In order to detect only the negative ions, we have modified an electron-impact spectrometer by adding a magnetic-field momentum filter.

A. Instrumental

A schematic diagram of the experimental setup is shown in Fig. 1. The basic spectrometer has been described in detail in a previous paper,[11] and only an outline will be given here. An electron beam emitted by a hairpin filament of thoria-coated iridium is energy selected by a 127° cylindrical electrostatic filter having a mean radius of 12.5 mm. The electron beam with the required energy spread is focussed onto the gas beam issuing from a tube with a 1-mm orifice, and the unscattered part is monitored on the electron collector. Negatively charged particles from the collision region are focussed onto the slit of a

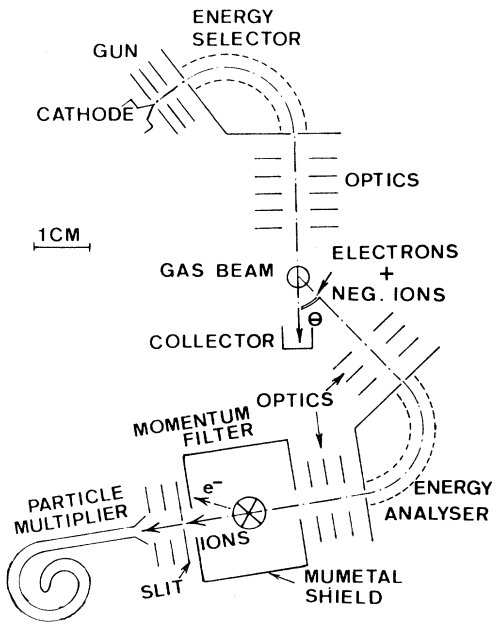

FIG. 1. Schematic diagram of the experimental set up.

second 127° electrostatic energy filter which can rotate about the scattering center for angles, with respect to the incident beam, between −10° and 135°. Particles leaving the energy analyzer enter the momentum filter assembly and are focussed on a 0.5 × 3 mm slit by a series of optics after having gone through a small magnetic field region. The optics have 5-mm-diam apertures and contain two split steering electrodes. Once through the slit the particles are detected by a tubular particle multiplier and the pulses are handled and stored in a multichannel scaler in the usual manner. The magnetic field is generated perpendicularly to the path of the particles and parallel to the slit by a small coil, 1-cm diameter, with about six turns, three on each side of the beam. The coil is wound onto a Mumetal yoke to limit stray fields and is further shielded by a Mumetal box so that the other elements of the instrument are unperturbed. With no current flowing in the coil, the instrument can be used in the usual modes of electron-impact spectroscopy.[11] In the presence of the magnetic field, the electrons with the lower momentum, but with the same energy as the ions, are deflected away from the slit and are no longer detected. The heavier ions are almost insensitive to the magnetic field; any slight deflection can easily be corrected by the steering electrodes so that they continue to be detected. Under usual working conditions and after optimization, a current of 0.8 A flows in the coil which generates a field of about 12 G. The cone potential of the particle multiplier is much higher than for electron detection, and saturation of the ion signal only occurs when this voltage approaches 1 kV.

Typically, in this study of CO, incident currents of 150 nA were used, which corresponds to an overall system resolution for electrons of about 100 meV, and a maximum ion count rate of 300 counts/sec for a background signal due to stray electrons reaching the particle multiplier of <1 counts/sec. The minimum detectable differential cross section (DCS) for negative-ion production under these conditions is $\sim 3 \times 10^{-22}$ cm^2/sr with a background gas pressure in the chamber not exceeding 1×10^{-4} Torr.

The instrument is made of a zinc-free nonmagnetic nickel-copper alloy, and the different elements can be baked out by coaxial heater wires. It is housed in a stainless-steel chamber which is oil-diffusion pumped. An in-vacuum Mumetal shield and Helmholz coils reduce external magnetic fields to less than 10 mG.

B. Operational modes

In the study of negative-ion fragments, the instrument can be used in modes similar to those for electron scattering.[11] An *ion-energy spectrum* can be obtained by maintaining the incident energy E_0 fixed and sweeping the energy analyzer potential. This produces a spectrum of the energy distribution of the negative-ion fragments, the peaks occurring at values of E_R given by Eq. (1).

The second mode leads to a *constant ion-energy spectrum* and is obtained by sweeping the incident energy and setting the energy analyzer to accept ions with a fixed energy E_R. Spectra are obtained with peaks occurring at incident energies E_0 satisfied by Eq. (1).

An *ion-yield spectrum* is produced by the third mode and indicates the yield of negative ions from a particular dissociation process as a function of electron energy and at a particular angle of observation. This is performed by setting E_0 and E_R so that they satisfy Eq. (1), and then sweeping the energy-selector and energy-analyzer voltages in such a way that their ratio remains constant and equal to $1:(1-\beta)$.

C. Energy scale calibration

The energy calibration of the incident beam was performed by two separate methods. The first technique was described in a previous Letter[12] and consists of, firstly, a plot of the energy position of the O^- ion peak formed by process I against the incident electron energy E_0. A straight line with a slope of $1-\beta = \frac{12}{28}$ is obtained, as expected from Eq. (1). Secondly, with the momentum filter inoperative so that electrons are detected, energy-loss spectra were recorded which show peaks resulting from excitation of the $b\,^3\Sigma^+$ and $B\,^1\Sigma^+ v=0$ levels. The energy locations of these peaks are then plotted against electron energy. Again straight lines are obtained but with a slope of unity as, for scattered electrons, $E_R = E_0 - E_n$ where E_n is the excitation energy of the state n. Such plots are shown in Fig. 2. The electron and ion plots cross and since, at the points of intersection, the residual energy for both ions and electrons is the same, then the absolute energy of the crossing points is known from the above equation and Eq. (1) and thus the shown energy scales are calibrated.

The second method uses the Feshbach resonance at 10.04 eV as a standard.[13] A constant residual energy spectrum of the scattered electrons, as shown in Fig. 3, is obtained by keeping the analyzer energy E_R fixed and sweeping the incident energy. A peak due to the resonance appears at 10.04 eV which immediately establishes the incident energy scale. The location of this structure is independent of E_R and is seen in the

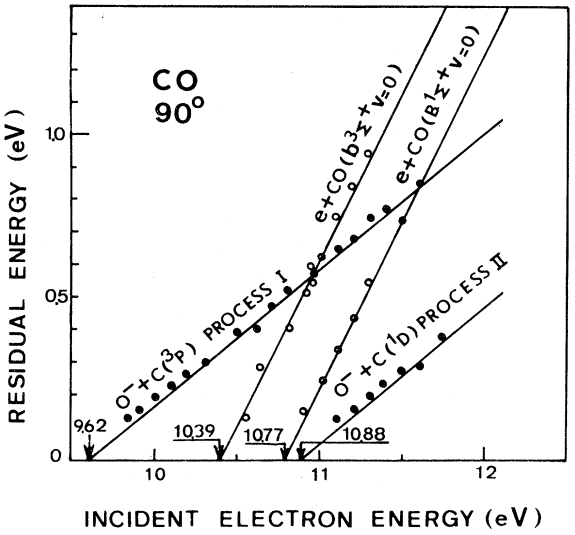

FIG. 2. Observed relative energies of the O^- ions and the electrons after excitation of the $b\,^3\Sigma^+$ and $B\,^1\Sigma^+$, $v=0$ levels with incident electron energy and at 90° scattering angle. The energy scale calibration is described in the text.

spectrum due to strong coupling of the resonance to high vibrational levels of the $A^1\Pi$, $a'\,^3\Sigma^+$, and, perhaps, $d\,^3\Delta$ states[13] which have an excitation energy of $(10.04 - E_R)$. The peak due to excitation of the $b\,^3\Sigma^+ v=0$ level appears on the incident energy scale at $E_0 = E_b + E_R$ which then calibrates E_R for the electrons.

The second method was used throughout this study as it is believed to be more accurate, in addition to being rapid and convenient. The error in the incident energy is estimated to be no greater than 50 meV. The latter method directly calibrates the incident energy and thus determines the energy available in the dissociating molecule. On the contrary, the first method depends on the observation of the post-collision energy of two very different particles which may not "see" the same contact potentials in the collision volume. Indeed, a discrepancy of about 0.1 eV was sometimes observed between the two calibration procedures. The O^- ions appeared to have less energy than would be expected from the calibration using the 10.04-eV resonance.

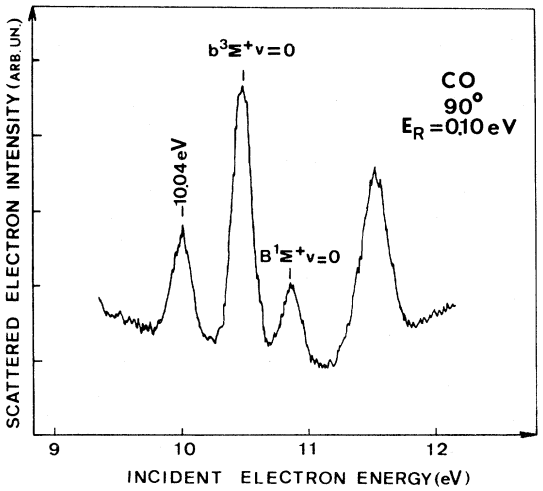

FIG. 3. Constant residual energy spectrum for electrons at a residual energy (E_R) of 0.10 eV and 90° scattering angle.

D. Thermal motion of target molecules

In electron-scattering experiments the thermal motion of the target particles has a negligible effect on the resolution which is currently available in electron-impact spectrometers. However, when the kinetics of the fragments of dissociation are being studied, as in the present experiment, the effect of the thermal motion dominates the resolution. Although the energy spread of the target molecules is only a few meV, conservation of momentum has the effect of amplifying this spread for the fragments so that the greater the fragment energy the broader its energy distribution. This subject has been treated by Chantry and Schulz,[14] who predict, for example, an energy spread, measured at half height of the distribution, of 400 meV for O^- ions from CO with a residual energy of 1 eV produced in a collision chamber at 300 °K. The present experiment uses a gas beam, and the effective temperature in the plane of analysis, perpendicular to the beam, is much lower. Typically, ion distributions with a width of ~160 meV were observed in CO for a fragment residual energy of 1 eV. This compares with a system resolution which can be as low as 20 meV for electron scattering. Thus the effect of the thermal motion is to produce broad peaks for the negative ions whose widths depend on their mean energy and, in the case of the third mode of operation where the ion yield is measured as a function of incident energy, leads to an underestimation of the ion signal as E_R increases.

E. Measuring procedure

Measurements of the angular behavior of the negative-ion intensity are performed in the following manner. Ion-energy spectra are obtained at a fixed incident energy and angle of observation. The negative-ion intensity is then taken as the peak height above the background. Such spectra are obtained at different angles, in series of four, and stored in separate quadrants of the multi-

channel analyzer, the first one always being recorded at 90° and to which the other peak heights are referred. In this way the effect of target pressure or incident current drifts, etc. are minimized as the instrument is quite stable during the time lapse of up to one hour required for these measurements. The four spectra obtained at different angles can be superimposed two by two or all together on the screen of the multiscalar. If there is a shift or a change in shape of the peak with angle, then the measurements are discarded as this signifies an inhomogeneous electrostatic potential in the collision region as the energy analyzer rotates. In this case baking the system, particularly the tube which forms the gas beam, is usually an effectively remedy. It was also verified that the magnetic field in the momentum filter did not perturb the collision center. An electron beam with an energy less than 1 eV was focussed into the collector, and it was noted that this current did not vary when the magnetic field was turned on at different angles. It can then be concluded that if the electrons are unaffected, then this must be the case even more so for the O^- ions, which have a momentum some thousand times greater at the same energy. Deformation of the angular distribution coming from other sources was also looked for by recording the angular behavior of O^- ions formed by dissociative attachment in O_2. As O_2 has like nuclei, a distribution symmetrical about 90° must always be obtained for the reasons put forward in Sec. II. Also O^- ions formed by the same process in NO were observed, and angular behaviors similar to those of Van Brunt and Kieffer[15,8] were measured.

F. Collision volume

The lack of an exact knowledge of the angular variation of the collision volume formed by the overlap of the incident electron beam, the gas beam, and the acceptance cone of the energy analyzer is a constant problem in obtaining accurate angular distributions.[11] This variation produces a deformation of the DCS and, in the worst case of a gas-filled collision chamber, the observed DCS must be corrected by $\sin\theta$, i.e., a 100% overestimation at 30° (and 150°). In electron scattering, the differential cross sections for elastic scattering from helium are well known[16] and can be used as an angular calibration. In our experience of electron scattering with the present instrument[11] where the collision volume is small, as the incident beam grazes the outlet of the gas-beam tube, the correction at all angles is small and never as dramatic as $\sin\theta$. For this study concerning negative ions, it will again be assumed that the correction is small although a pessimistic correction of $\sin\theta$ will be taken into account when estimating the error.

G. Gas purity

Carbon monoxide gas of 99.99% purity was employed. The use of a flowing gas beam should maintain this purity in the collision region since the background pressure, without the beam, is better than 10^{-7} Torr. The observed ion peaks have a behavior with electron energy corresponding to O^- ions from CO as shown in Fig. 2; no trace of other ions was observed although no high-resolution mass analysis was performed.

IV. RESULTS

Examples of the different modes of operation of the instrument, described in Sec. III and applied to negative-ion formation through dissociative attachment in CO, are shown in Figs. 4 to 7. Figure 4 shows ion-energy spectra taken at an incident energy of 11.1 eV and observation angles of 40°, 90°, and 130°. Two peaks are revealed corresponding to the two processes. Figure 2 shows the energetic positions of the peaks as a function of electron energy and, as described earlier, they present the correct behavior for

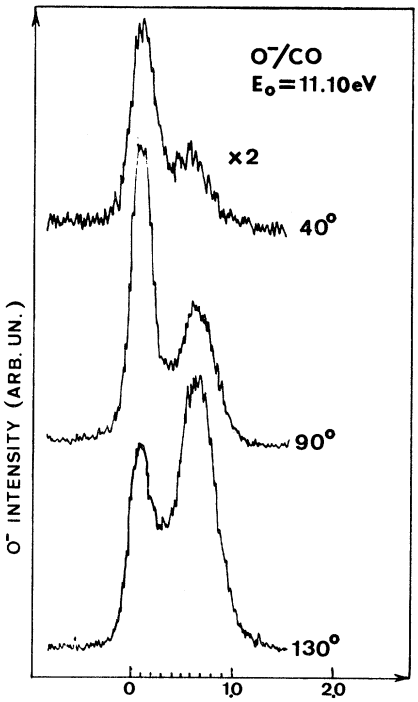

FIG. 4. Ion-energy spectra for O^- ions at an incident electron energy (E_0) of 11.10 eV taken at 40°, 90°, and 130°.

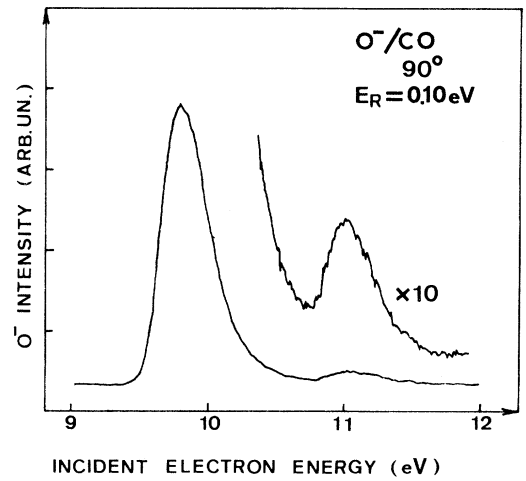

FIG. 5. Constant-ion-energy spectrum for O^- ions at 0.10 eV residual energy (E_R) and 90°. Same conditions and technique as the spectrum of Fig. 3 but with momentum filter operating.

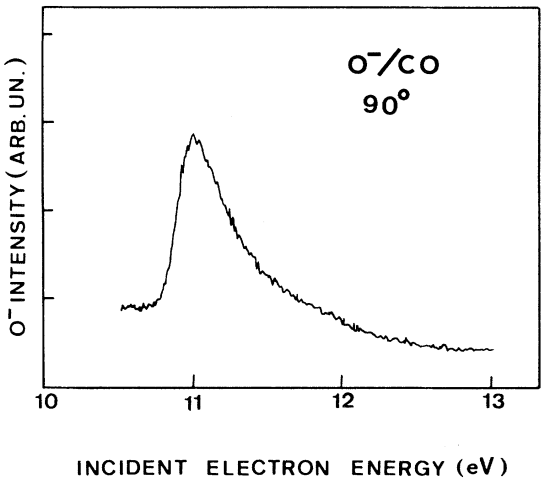

FIG. 7. Ion-yield spectrum for O^- ions from process II at 90° taken with the analyzer optics tuned to zero fragment energy and E_0 and E_K varied simultaneously to satisfy Eq. (1).

O^- ions from CO. The lower energy peak corresponds to process II and the higher one to process I. The relative intensity of the first to second peak is not significant, the DCS's for process I are the larger at this energy (see below) but for these spectra, the collection of low-energy ions is favored by the tuning of the energy-analyzer optics, thus enhancing the peak intensity of process II. The peak widths differ for the two processes. This clearly illustrates the domination of the thermal motion of the target particles in determining the resolution and its dependence on fragment energy. Also there is a strong difference in angular behavior of the peak intensities. The peak from process II is highest at 90°, whereas that from process I increases with scattering angle.

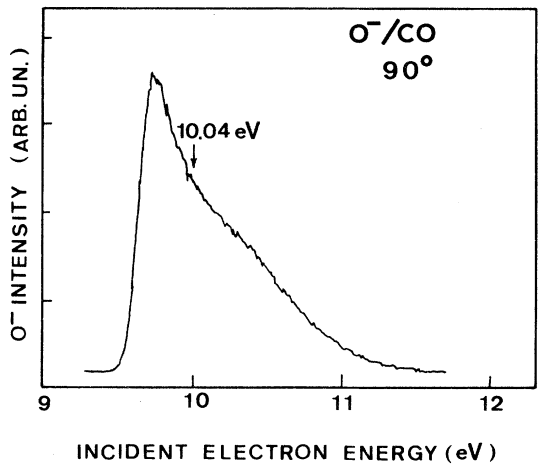

FIG. 6. Ion-yield spectrum for O^- ions from process I at 90° taken with the analyzer optics tuned to zero fragment energy and E_0 and E_K varied simultaneously to satisfy Eq. (1).

A constant-ion-energy spectrum is shown in Fig. 5 for a scattering angle of 90° and a fixed ion energy of 0.1 eV. The experimental conditions and technique used are exactly the same as for the electron spectrum shown in Fig. 3 except the magnetic field of the momentum filter is turned-on. Peaks produced by O^- ions from the two processes are clearly visible. The peak separation is measured to be 1.25 ± 0.03 eV which compares well with the accepted energy between thresholds of 1.26 eV. The experimental peaks are broad and asymmetrical with a relatively sharp rise and a tailing off on the high-energy side. For the first peak, the width from half height to maximum of the onset is 60 meV whereas the width from maximum to half height of the decay is 110 meV, both measured on the ion energy scale, i.e., the incident electron scale multiplied by $1-\beta=\frac{12}{28}$. The instrumental resolution for this spectrum is about 100 meV. All the above peak characteristics can be understood in terms of the fragment energy spread and its increase with fragment energy introduced by the thermal distribution of the target molecules.

The relative peak heights represent the ratio of the DCS's for the two processes at the same energy, i.e., $E_R(1-\beta)^{-1}$, above their respective dissociation thresholds. At 90° the process I to II peak height ratio showed a slight increase with

ion energy. For $E_R = 0.05$ eV, a factor of 15 ± 5 rising to 18 ± 6 at 0.1 eV and 22 ± 8 at 0.3 eV was obtained. As will be seen below, the angular behavior of the DCS's of the two processes are only weakly dependent on energy; hence these factors can be taken as the integral cross-section ratios and would indicate a slightly shallower potential curve for process II compared to process I. However, not too much faith should be placed in such a conclusion as, in the dissociation of short-lived molecular negative ions, the survival probability of the resonance can vary with internuclear distance and must be taken into account.

An ion-yield spectrum for process I at 90° is shown in Fig. 6. The rise of the curve is in agreement with a vertical onset convoluted with an experimental resolution of 100 meV, and the threshold, taken at the point of steepest slope, agrees well with the accepted value of 9.62 eV. The shape of the decaying curve does not represent the energy dependence of the DCS. In order to obtain a good onset the energy-analyzer optics are tuned to zero fragment energy and the collection efficiency decreases rapidly as the ion energy rises. Also, as discussed earlier, the thermal motion of the target particles broadens the distribution with increasing energy which leads to an underestimation of the ion yield away from threshold.

A very weak structure can be noticed in the region of 10.04 eV and the Feshbach resonance at this energy can be the cause. The sharp resonance has Σ symmetry[13] and that of the dissociating state is expected to be Π (see Sec. V). Thus, any perturbation must take place through rotational coupling between the two states and is probably a very small effect, which is consistent with these observations.

Figure 7 shows an ion-yield spectrum for process II taken under similar experimental conditions to those used for that of process I. The onset corresponds to the instrumental resolution of 100 meV and thus again indicates a vertical threshold for the process. The onset, taken at the point of steepest slope, is in accordance with a threshold energy of 10.88 eV. The sloping background is caused by O^- ions from process I which are detected due to the incomplete separation of ions from the two processes imposed by the thermal broadening.

The angular behavior of the O^- ion intensity for process I at incident electron energies of 9.85 eV, 10.6 eV, and 11.2 eV are shown in Fig. 8. The error bars represent an appreciation of the error with respect to the peak at 90° and contain an estimation of the statistical scatter as well as the full $\sin\theta$ correction. As mentioned in Sec. III, this geometrical correction is very pessimistic and,

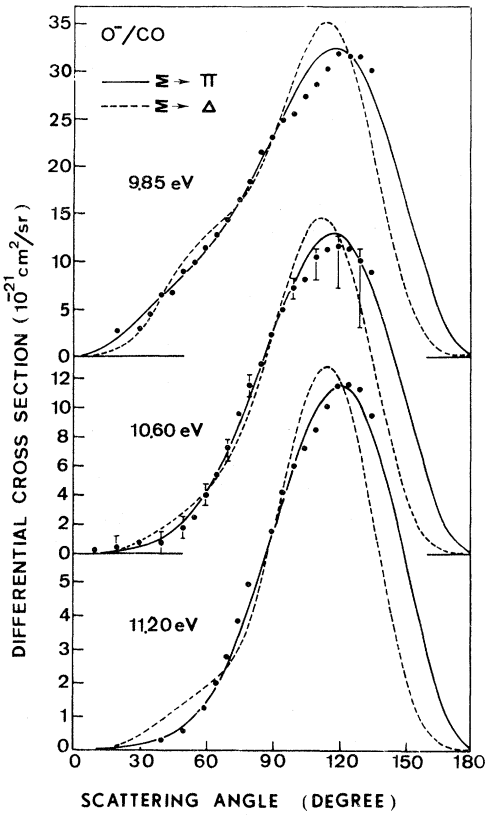

FIG. 8. Differential cross sections for O^- ions from process I at incident energies of 9.85, 10.60, and 11.20 eV. The curves represent the best fits of a theoretical expression for the indicated transitions to the experimental points.

in past experience, the correction at 135° in electron-scattering experiments is rarely greater than 0.9 whereas $\sin 135° = 0.71$.

The angular behaviors of the DCS's at 10.6 eV and 11.2 eV were placed on an absolute scale by integration of the theoretical expression for the best fit (see below) and normalization to the absolute integral values of Rapp and Briglia.[4] The cross-section curve of Rapp and Briglia[4] is strongly rounded near threshold due to the low instrumental resolution, and their cross section at 9.85 eV is lower than at the maximum which they observe to occur at a higher energy. The cross section should peak at threshold (9.62 eV) in the absence of instrumental distortion and that observed by Chantry,[3] with a better resolution, has a steeper onset than the curve of Rapp and Briglia[4] but with the same decay. Consequently the 9.85-eV DCS angular dependence was normalized to the value of $2.62 \times 10^{-3}\ \Pi a_0^2$ obtained from the curve of Chantry[3] normalized to the absolute value of Rapp and Briglia[4] at 10.6 eV.

When limited to two partial waves, Eq. (3) has the form $\sigma(\theta) \sim |Y_{L\mu} + AY_{L+1\,\mu}|^2$ where A is complex and equal to the ratio of the matrix elements $a_{L+1\,\mu}/a_{L\mu}$. Process I results in $O^-(^2P)$ and $C(^3P)$ and hence can take place through resonant states with Σ, Π, and Δ symmetry. As the CO ground state has Σ symmetry, the above relation has the following explicit forms for the three possible transitions:

$$\Sigma \to \Sigma\,, \sigma(\theta) \sim (1 + 3.46A_1A_2\cos\theta + 3A_1^2\cos^2\theta)\,,$$

$$\Sigma \to \Pi\,, \sigma(\theta) \sim \sin^2\theta(1 + 4.47A_1A_2\cos\theta + 5A_1^2\cos^2\theta)\,,$$

$$\Sigma \to \Delta\,, \sigma(\theta) \sim \sin^4\theta(1 + 5.29A_1A_2\cos\theta + 7A_1^2\cos^2\theta)\,,$$

where A_1 is the modulus of A and A_2, the cosine of the argument. These expressions were fitted to the angular dependencies and the results for Π and Δ resonance symmetries are shown in Table I and Fig. 8. Γ represents the quality of the fit and is the standard deviation defined by

$$\Gamma = \left(\frac{1}{N}\sum_{i=1}^{N}[\sigma_{\mathrm{calc}}(\theta_i) - \sigma_{\mathrm{expt}}(\theta_i)]^2\right)^{1/2}.$$

This criterion was chosen as it is well adapted to the present problem. In this formula the statistical weight of the DCS's at low angles is small because the observed DCS's are small in this region. As discussed earlier, any volume correction would only be appreciable at these small angles; thus the incidence of such a correction on the fitting procedure is reduced.

A $\Sigma \to \Sigma$ transition gave a best fit which bore no relation to the experimental results and is not represented here. This would be expected from Dunn's rules[6] which indicate that the DCS should not go to zero at 0° (and 180°) as it would appear to do here.

The angular behaviors of the DCS for process II at 11.1 and 11.4 eV are displayed in Fig. 9 and a more symmetrical behavior with respect to 90°,

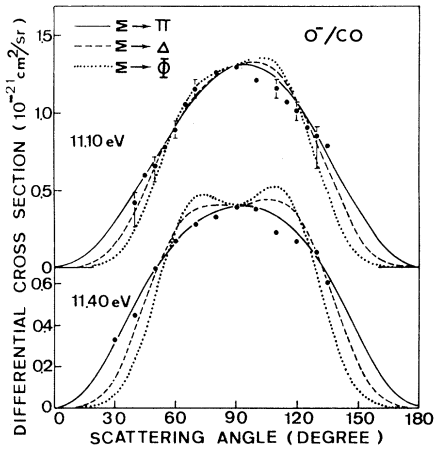

FIG. 9. Differential cross sections for O^- ions from process II at 11.10 and 11.40 eV incident electron energies. The curves represent the best fits of a theoretical expression for the indicated transitions to the experimental points.

compared to process I, is apparent. The error bars were determined in the same way as for process I. The absolute cross-section scale was obtained by normalization to process I using the relative values obtained from constant ion-energy spectra, taken at 90°, such as that of Fig. 5. The error with respect to process I is quite large, about ±30%, and is not contained in the error bars.

Process II yields $O^-(^2P)$ and $C^*(^1D)$ which can originate from resonance states with Σ, Π, Δ, and Φ symmetry. The functions written above for transitions to the first three of these states were fitted to the experimental results along with that for a $\Sigma \to \Phi$ transition which has the form:

$$\sigma(\theta) \sim \sin^6\theta(1 + 6.00A_1A_2\cos\theta + 9A_1^2\cos^2\theta)\,.$$

The results for the best fits are shown in Table II and Fig. 9. Again a $\Sigma \to \Sigma$ transition is not ex-

TABLE I. Dependence of the fitting parameters on incident electron energy and resonance state symmetry for process I. Γ is the standard deviation.

Electron energy (eV)	Resonance state	A_1	A_2	Γ
9.85	Π	0.45	−0.60	0.05
	Δ	0.67	−0.45	0.13
10.60	Π	0.35	−0.98	0.04
	Δ	0.55	−0.70	0.13
11.20	Π	0.45	−0.94	0.05
	Δ	0.65	−0.72	0.18

TABLE II. Dependence of the fitting parameters on incident electron energy and resonance state symmetry for process II. Γ is the standard deviation.

Electron energy (eV)	Resonance state	A_1	A_2	Γ
11.10	Π	0.07	−0.46[a]	0.04
	Δ	0.45	−0.08	0.07
	Φ	0.60	−0.06	0.11
11.40	Π	0.32	−0.04	0.04
	Δ	0.60	−0.02	0.09
	Φ	0.72	−0.02	0.16

[a] Unreliable since $A_1 \sim 0$; see text.

pected from Dunn's rules[6] as the DCS's go to zero at 0° (also presumably at 180°) and indeed gave an unrealistic fit which is not shown.

V. DISCUSSION

A. Process I

It is apparent from Table I and Fig. 8 that a $\Sigma \rightarrow \Pi$ transition consistently gives the best fit to the angular dependencies of the DCS for O^- ion formation through process I. The fitting technique with two partial waves produced unique results. It is reasonable to suppose that the two lowest-allowed partial waves are sufficient to describe the observed angular distributions in the case of CO. Table I shows that the amplitudes for the second partial wave is already much reduced with respect to the first and the third can be expected to be appreciably smaller. Moreover, the DCS values at small angles are dominated by the $\sin^{2L}\theta$ factor which would remain unaffected by the addition of a third partial wave. A $\Sigma \rightarrow \Pi$ transition not only gives the best overall fit but also produces the best agreement at small angles.

As was mentioned earlier, there are two reasons for rapid convergence of expansion (3). By inspecting the coefficients of the expansion obtained using the simple plane-wave model of Van Brunt,[17] one can see that the first two terms are dominant especially for $\Sigma \rightarrow \Delta$ and $\Sigma \rightarrow \Phi$ transitions. As pointed out by Van Brunt and Kieffer,[15] this explains why there is almost no difference between the curves fitted to O^- distributions from NO for $\Pi \rightarrow \Sigma$ and $\Pi \rightarrow \Delta$ transitions as they only differ by the third and higher members of the expansion. We also expect, for carbon monoxide, that the expansion of ϕ_r in spherical harmonics will converge rapidly and that this will considerably reinforce the convergence of expansion (3).

The angular dependencies of the DCS's are almost independent of electron energy over a wide range. This indicates that a single Π state is responsible for the dissociative attachment reaction. Also, it is obvious from spin conservation in this light molecule, that this state must be a doublet as the ground state of CO is a singlet. The parameters A_1 and A_2 vary slowly from 10.6 to 11.2 eV but are somewhat different from those at 9.85 eV. The angular distribution measured at 9.85 eV is expected to be the least reliable as the fragment residual energy is very low ($E_R = 0.10$ eV) and there may be a systematic error due to a slight potential penetration into the scattering region which could alter the angular behavior. Nevertheless we are confident that the general shape and the backward peaking are correct at this energy as they are reproducible under many different experimental conditions.

The value of $A_2 \sim -1$ indicates a strong deformation of the electron wave function from a plane wave ($A_2 = 0$) and reflects the asymmetry with respect to 90°. This is in contrast with the only angular observation of dissociative attachment in a heteronuclear diatomic (NO)[15] where, within experimental error, only distributions with forward-backward symmetry were observed and plane-wave theory accounted for the experimental results.

The carbon atom and the oxygen ion in their ground states (P) can form two $^2\Pi$ states. The lower is the well-known shape resonance associated with the CO ground state and is centered at 1.8 eV. As far as we are aware, no calculations have been performed to determine the energy location of the CO^- states; however CO^- is isoelectronic with NO, and a comparison with the states of this molecule can help indicate the configuration of the resonance. The $^2\Pi$ ground state of NO has a $\sigma^2\pi^4\pi$ configuration and corresponds to the low-lying shape resonance of CO. The lowest excited $^2\Pi$ state of NO is the B state[18] at 5.7 eV which is bound in the Franck-Condon region as the CO^- resonant state must also be, as indicated by the vertical onset of the O^- production curve. The second excited $^2\Pi$ state is the L state[18] situated about 2 eV above the B state and is also bound in the Franck-Condon region. Both of these states have the same dominant configuration of $\sigma^2\pi^3\pi^2$. Consequently we would propose that the resonance state responsible for process I also has a $\sigma^2\pi^3\pi^2$ configuration and is most probably the analog of the lower of these two states, namely, the $B\,^2\Pi$ state.

Thus the resonance would be formed by adding the incident electron in a π orbital to an excited parent state of CO with a $\sigma^2\pi^3\pi$ configuration. Excitation of this parent state should be prominent under electron impact. The resonance, necessarily of the shape type, which leads to dissociative attachment, also couples to the parent state by a one-electron transition into the continuum. The latter process is strongly favored, producing increased cross sections, as this electronic process is fast compared to the dissociation process. The most prominent state of CO with this configuration excited by electron impact is the $a'\ ^3\Sigma^+$ state, as was shown by Mazeau *et al.*[13] and Swanson *et al.*[19] Indeed excitation functions of different vibrational levels of this state[19] show resonance enhancement of the cross section in the vicinity of the first dissociation limit for the formation of O^- (9.62 eV). The resonant structure in these channels is particularly broad and structureless; this is typical of shape resonances which are very short lived, and they are well-

described theoretically by the impulse model. They have a lifetime of $\sim 10^{-15}$ sec whereas dissociation typically takes more than 10^{-14} sec. A survey of the observations of Swanson *et al*[19] and a comparison with integral cross sections for excitation of the $A\,^1\Pi$ state obtained optically[20] would indicate a cross section of roughly 10^{-17} cm^2 for $a'\,^3\Sigma^+$ state excitation at 10 eV. The peak value for dissociative attachment is 3×10^{-19} cm^2, and the ratio to the $a'\,^3\Sigma^+$ state cross section is of the same order as the ratio of the dissociation time to the resonance lifetime, which is not inconsistent with the choice of the $a'\,^3\Sigma^+$ state as parent.

The $a'\,^3\Sigma^+$ state has a large permanent dipole moment which has been measured experimentally to have the value of -1.05 D (C^-O^+).[21] This could account for the strong distortion of the electron wave function during formation of the resonant state. Furthermore, as the concentration of the valence electron in the a' state is mainly on the carbon atom, the incident electron will prefer to attach to the oxygen atom to form O^-, and one can imagine that it will choose orientations of the molecule with the oxygen atom towards the incident direction, hence producing the backward peaking of the O^- distribution.

The $a\,^3\Pi$ and the $A\,^1\Pi$ states are also strongly excited near the O^- formation threshold and excitation functions of their vibrational levels show much resonant structure. These states have a $\sigma\pi^4\pi$ configuration and can form a resonance by attaching an electron into a π orbital to compose, other than Σ states, a $^2\Delta$ state equivalent to the $B'\,^2\Delta$ state of NO. This is the only known valence state in NO with Δ symmetry and is bound in the Franck-Condon region. It could be possible for this state of CO^- to lead to the formation of O^- ions. However, as the results show, a $\Sigma \rightarrow \Delta$ transition gives worse fits than those for $\Sigma \rightarrow \Pi$ and, in addition, the $a\,^3\Pi$ state has a large positive dipole moment of +1.38 D (C^+O^-)[22] and, using the simple reasoning above, would lead preferentially to C^- formation and, eventually, to a forward-peaking angular distribution for O^- ions which is not the case in this experiment.

B. Process II

The angular distributions of O^- ions measured for process II with a threshold at 10.88 eV are very similar at the two energies of observation. Here the curves are more symmetrical about 90° than those for process I although backward ejection is still slightly favored. Table II indicates that the symmetry of the intermediate state is most probably Π and it must also be a doublet from spin conservation. The arguments put forward above supporting a two partial-wave analysis, are also relevant in this case. The fit for Δ and Φ states are less satisfactory and the lobes on the fitted curves are not reproduced by the experimental observations. At 11.10 eV, A_1 is small and indicates that the $p\pi$ partial wave is almost pure, consequently A_2 cannot be determined accurately and its value here has little meaning. Indeed a fit with $p\pi$ alone, i.e., $\sigma(\theta) \sim \sin^2\theta$, yielded $\Gamma = 0.06$ which is better than the fits for either Δ or Φ states using two partial waves. At 11.40 eV the value of A_1 indicates an increasing contribution from the $d\pi$ partial wave, as would be expected as one moves away from threshold. Here A_2 is meaningful and indicates that there is virtually no distortion of the incident wave function.

As for process I, the O^- onset curve is vertical indicating a bound potential curve in the Franck-Condon region for the CO^- state. Again with reference to NO and, as mentioned above, the second $^2\Pi$ excited state of NO is the $L\,^2\Pi$ state at 7.6 eV which has a $\sigma^2\pi^3\pi^2$ configuration. No other bound valence $^2\Pi$ states higher than the L state have been observed.[23] Calculations of the potential curves of NO valence states by Thulstrup *et al*.[24] gave bound potential curves for the B and the L states; all the other $^2\Pi$ states were repulsive in the Franck-Condon region. Similarly, calculations of the valence states of PO[25] which has the same valence shell configuration as CO^-, gave the two lowest excited $^2\Pi$ states as bound and a third much higher one as repulsive, all three states having the same dominant configuration, namely $\sigma^2\pi^3\pi^2$. Consequently, in the light of these observations, it is probable that the configuration of the resonance is also $\sigma^2\pi^3\pi^2$. As for process I, the parent state would have a $\sigma^2\pi^3\pi$ configuration. No state with this configuration other than the $a'\,^3\Sigma^+$ state have been observed in electron-impact spectroscopy experiments. However, using a more sensitive optical technique, Skubenich[26] detected electron-impact excitation of the $d\,^3\Delta$ state and measured a maximum cross section near threshold of 5×10^{-18} cm^2. This could be a possible candidate for the parent state of the resonance. The experimental results indicate that if the dipole moment of this state is responsible for the electron wave distortion, then it should be very small; however this quantity essentially depends on the configuration and as the $\sigma^2\pi^3\pi$ configuration in the case of the $a'\,^3\Sigma^+$ state yields a strong dipole moment then a similar situation would be expected to exist for the $d\,^3\Delta$ state.

The resonance could also possibly be a $^2\Delta$ state although this is ruled out by the fitting procedure. The only known $^2\Delta$ state in NO is the B' state

mentioned above, which dissociates to the first O^- limit. Two $^2\Delta$ states can lead to $C^*(^1D)$ and $O^-(^2P)$ but their analogs in NO are unobserved, and the calculations on PO[25] did not reveal a bound $^2\Delta$ state other than the analog of the B state. Thus, the absence of bound $^2\Delta$ states would reinforce the assignment of Π symmetry to the resonant state of process II.

VI. CONCLUSION

Two separate dissociative attachment reactions lead to the formation of O^- ions in CO. The dominant process yields the O^- ion and the carbon atom in their ground states. The experimental evidence and the analysis of the angular behavior of the O^- intensity by means of an expansion of the differential cross section, limited to the first two allowed partial waves, indicates that the dissociating CO^- state, responsible for this process, has Π symmetry and is bound in the Franck-Condon region. A comparison with isoelectronic NO leads almost unambiguously to the choice of a $\sigma^2\pi^3\pi^2$ configuration for the resonant state. The parent state of the resonance then has a $\sigma^2\pi^3\pi$ configuration and there is reason to believe that it is the $a'\,^3\Sigma^+$ state from a survey of electron-scattering experiments on CO. Also the strong dipole moment of the $a'\,^3\Sigma^+$ state could account for the distorted electron wave and maybe explain the forward-backward asymmetry of the O^- differential cross section.

The second process leads to a carbon atom in the first excited state in addition to a ground-state O^- ion. Here also a $^2\Pi$ resonance state, bound in the Franck-Condon region, is indicated by the evaluation of the experimental results. As for the first process $\sigma^2\pi^3\pi^2$ seems probable for the resonance configuration by analogy with NO. The parent state with a $\sigma^2\pi^3\pi$ configuration is tentatively proposed to be the $d\,^3\Delta$ state of CO.

ACKNOWLEDGMENTS

The authors are grateful to Florence Fiquet-Fayard and Hélène Lefebvre-Brion for most helpful discussions. One of us (I.Č.) is grateful to the CNRS of France for a one month grant provided through the exchange program with the RZNR of SR Serbia.

---

*Permanent address: Institute za Fiziku, Studentski trg 16/V, 11000 Beograd, Yugoslavia.

†Permanent address: Laboratoire de Collisions Electroniques, Université Paris-Sud, 91405 Orsay, France.

‡Equipe de Recherche Associée au C.N.R.S.

[1]W. W. Lozier, Phys. Rev. 36, 1285 (1930).

[2]A. L. Vaughan, Phys. Rev. 38, 1687 (1931).

[3]P. J. Chantry, Phys. Rev. 172, 125 (1968).

[4]D. Rapp and D. D. Briglia, J. Chem. Phys. 43, 1480 (1965).

[5]A. Stamatović and G. J. Schulz, J. Chem. Phys. 53, 2663 (1970).

[6]G. H. Dunn, Phys. Rev. Lett. 8, 62 (1962).

[7]T. F. O'Malley and H. S. Taylor, Phys. Rev. 176, 207 (1968).

[8]R. J. Van Brunt and L. J. Kieffer, Phys. Rev. A 2, 1899 (1970).

[9]R. de L. Kronig, Z. Phys. 50, 347 (1928).

[10]S. Trajmar and R. I. Hall, J. Phys. B 7, L458 (1974).

[11]R. I. Hall, G. Joyez, J. Mazeau, R. Reinhardt, and C. Schermann, J. Phys. (Paris) 34, 827 (1973).

[12]I. Čadež, M. Tronc, and R. I. Hall, J. Phys. B 8, L73 (1975).

[13]J. Mazeau, F. Gresteau, G. Joyez, J. Reinhardt, and R. I. Hall, J. Phys. B 5, 1890 (1972).

[14]P. J. Chantry and G. J. Schulz, Phys. Rev. 156, 134 (1967).

[15]R. J. Van Brunt and L. J. Kieffer, Phys. Rev. A 10, 1633 (1974).

[16]D. Andrick and A. Bitsch, J. Phys. B 8, 393 (1975).

[17]R. J. Van Brunt, J. Chem. Phys. 60, 3064 (1974).

[18]F. R. Gilmore, J. Quant. Spectrosc. Radiat. Transfer 5, 369 (1965).

[19]N. Swanson, R. J. Celotta, C. E. Kuyatt and J. W. Cooper, J. Chem. Phys. 62, 4880 (1975).

[20]M. J. Mumma, E. J. Stone, and E. C. Zipf, J. Chem. Phys. 54, 2627 (1971).

[21]B. G. Wicke, R. W. Field, and W. Klemperer, J. Chem. Phys. 56, 5758 (1972).

[22]R. S. Freund and W. Klemperer, J. Chem. Phys. 43, 2422 (1965).

[23]E. Miescher, *M. T. P. International Review of Sciences (Spectroscopy)* Phys. Chem. Series II, Vol. III (to be published).

[24]P. W. Thulstrup, E. W. Thulstrup, A. Andersen, and Y. Ohrn, J. Chem. Phys. 60, 3975 (1974).

[25]A. L. Roche and H. Lefebvre-Brion, J. Chem. Phys. 59, 1914 (1973).

[26]V. V. Skubenich, Opt. Spektrosk. 23, 990 (1967) [Opt. Spectrosc. 23, 540 (1967)].